ISSN 1810-2328, Journal of Engineering Thermophysics, 2019, Vol. 28, No. 3, pp. 410–430. © Pleiades Publishing, Ltd., 2019.

Effect of Internal Heat Generation and Concentration Change on Free Convection Boundary Layer from Vertical Flat Plate Embedded in Porous Medium

R. Akter[1*], M. Ferdows[2], and A. Miyara[3,4]

[1]*Department of Mechanical Engineering, Graduate School of Science and Engineering, Saga University, 1 Honjomachi, Saga-shi 840-8502, Japan*

[2]*Research Group of Fluid Flow Modeling and Simulation, Department of Applied Mathematics, University of Dhaka, Dhaka-1000, Bangladesh*

[3]*Department of Mechanical Engineering, Faculty of Science and Engineering, Saga University, 1 Honjomachi, Saga-shi 840-8502, Japan*

[4]*International Institute for Carbon-Neutral Energy Research, Kyushu University, Fukuoka-shi 819-0395, Japan*

Received June 6, 2018; in final form, June 20, 2019; accepted July 2, 2019

Abstract—The effects of exponentially decaying internal heat generation (IHG) and internal mass generation (IMG) over specific components are presented numerically on coupled heat and mass transfer by a free convection boundary layer over a vertical flat plate embedded in a fluid-saturated porous medium. Corresponding similarity solutions are used to reduce the governing partial nonlinear differential equations to three ordinary differential equations for the dimensionless stream function, temperature, and concentration with the following parameters: buoyancy force N, exponent of x, λ, and Lewis number Le. Media with and without IHG and IMG are compared in context with the help of graphs and tables. Computations are performed with a system of parameters using built-in codes in Maple. The influences of these parameters on velocity, temperature and concentration profiles, and Sherwood and Nusselt numbers are thoroughly compared and graphically illustrated.

DOI: 10.1134/S1810232819030111

1. INTRODUCTION

Boundary layer flow induced by a heated vertical plate that is embedded in a porous medium has several industrial applications and advancements. The functional applications are in an assortment of engineering procedures, such as relocation of dampness in heat exchangers, petroleum reservoirs, filtration, chemical catalytic reactors and processes, nuclear waste vaults, spreading of synthetic contaminations in plants, diffusion of drugs in blood veins, and extraction of geothermal energy. Coupled heat and mass transfer on a vertical surface is important from practical and theoretical perspectives due to their extensively valuable applications in the cooling of electronic supplies, heat exchange from refrigeration curls, heat loss from power transmission lines, and heat exchange from humans and bodies of creatures. Moreover, coupled heat and mass transfer can explain certain regular phenomena, such as sea streams driven by differential heating and serve as cargo trains for salt, as specified by Bejan (1993), and the part of manufacturing plants that squanders gas dissemination in a differential heating coursed air. This reality has inspired a few scientists to examine the impact of coupled heat and mass transfer.

Nield and Bejan [1] and Ingham and Pop [2] exhaustively examined convection through permeable media. The similarity method of Darcy's model with boundary layer assumptions of steady free convection about a vertical plate embedded in porous media was contemplated by Cheng and Minkowycz [3]. Reference number [3] extended by Cheng [4] by considering the influence of lateral mass flux with support for the power law variations of temperature and velocity on a vertical surface. By using power

*E-mail: rabeya.ju@gmail.com

law forms, Johnson and Cheng [5] accounted for the fundamental and adequate conditions under which similarity solutions exist for free convection boundary layers adjacent to flat plates in porous media. A few researchers [6–9] concluded that similarity solutions exist for Darcy and Boussinesq approximations and that these solutions are comparable for a few porous medium cases according to the power law forms of velocity and temperature between the wall and environments. Magyari and Keller [10] reported the exact analytical solutions required in determining the effect of lateral mass flux on natural convection boundary layers induced by a heated vertical plate embedded in a saturated porous medium. In their exact analytical solutions, they considered certain power law variations of temperature index $\lambda = 1, -1/3$, and $-1/2$ and found that solutions can only exist for suction ($f > 0$) for $\lambda = -1/2$, suggesting that this condition is suction-born. In the presence of exponentially decaying internal heat generation (IHG), Crepeau and Clarksean [11] revealed a new type of similarity solutions for isothermal vertical plates in semi-infinite quiescent fluids. Without a heat generation term, Merkin and Zhang [6] found that the parameter m should fulfill the range $\lambda > -2/5$ for flat plates in permeable media. Meanwhile, Ingham and Brown [5] presented that for vertical surfaces in permeable media, a solution exists only for $\lambda > -1/2$. Postelnicu and Pop [12] utilized the same source capacity with power law variation of temperature distribution to consider the boundary layers developed by heated vertical and flat plates in porous media. The work of [12] was extended by Postelnicu et al. [13] to porous vertical plates. In the presence of IHG, Grosan and Pop [14, 15] developed a natural convection boundary layer using a vertical flat surface in a porous medium for a non-Newtonian fluid. Furthermore, a similarity solution for a natural convection boundary layer with an IHG term over an arbitrary shape, which is an axisymmetric body embedded in a permeable medium, was presented by Bagai [16].

With reference from Crepeau and Clarksean [11] and Postelnicu and Pop [12], a similarity solution for a fluid with exponentially decaying heat and mass generation terms over a specific component and a constant temperature vertical plate is developed. The present study extends these references to investigate the effect of IHG and IMG over a specific component on the boundary layer. This approach is new in the area encompassed by the present work. An exponential form is used for the internal energy and mass generation terms over a specific component. All the numerical solutions are obtained through the use of the software Maple. The procedure used to solve the resultant differential equations is validated by the acquisition of the solutions for a constant temperature vertical plate without IHG and IMG, as shown in the figures.

2. PROBLEM FORMULATION

We consider the two-dimensional (2D), viscous, laminar, and steady free convection boundary layer flow induced by a heated vertical plate. The 2D diagram considered is depicted in Fig. 1. The plate is assumed embedded in a homogeneous porous medium of uniform ambient temperature T_∞ and with IHG q''' and IMG q'''_m over a specific component. The Darcy–Boussinesq approximation holds, and the temperature distribution of the heat varies as x^λ. The governing conservation equations of this boundary layer flow for incompressible viscous fluid are as follows [1]:

$$\frac{\partial u}{\partial x} + \frac{\partial v}{\partial y} = 0, \tag{1}$$

$$\frac{\partial u}{\partial y} = -\frac{g\beta K}{\upsilon}\left(\frac{\partial T}{\partial x} + \frac{\partial C}{\partial x}\right), \tag{2}$$

$$u\frac{\partial T}{\partial x} + v\frac{\partial T}{\partial y} = \alpha\frac{\partial^2 T}{\partial y^2} + q''', \tag{3}$$

$$u\frac{\partial C}{\partial x} + v\frac{\partial C}{\partial y} = D\frac{\partial^2 C}{\partial y^2} + q'''_m, \tag{4}$$

where u, v, T, and C are the fluid x-component of velocity, y-component of velocity, temperature, and concentration, respectively. The symbols υ, g, β, and K correspond to the kinematic viscosity, gravitational acceleration, thermal expansion coefficient, and permeability of the porous medium, respectively.

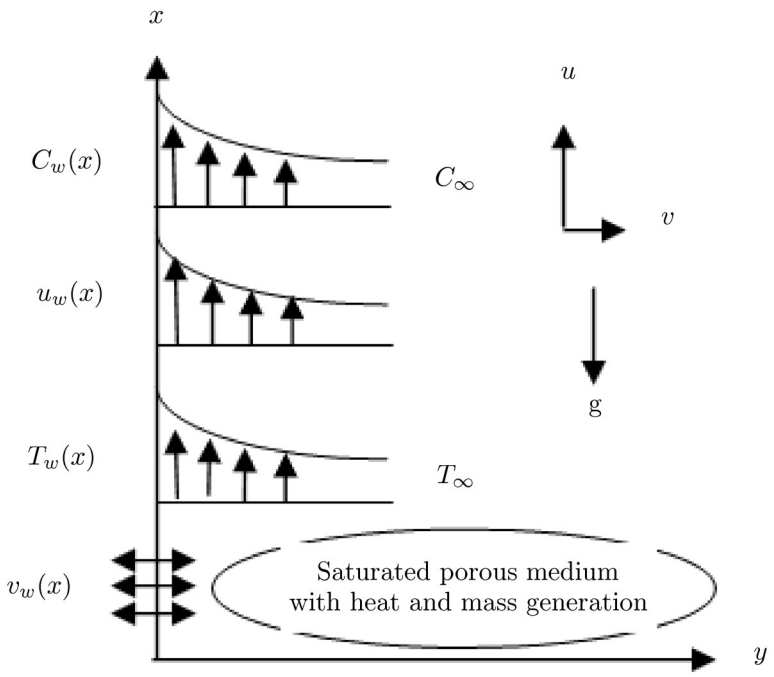

Fig. 1. Schematic diagram and coordinate system.

The symbols α, D, q''', and q'''_m stand for thermal diffusivity, mass diffusivity, IHG rate, and IMG rate over a specific component, respectively. The wall temperature and concentration are assumed to have power law variation forms, as shown by the following equations:

$$T_w(x) = T_\infty + Ax^\lambda \quad \text{and} \quad C_w(x) = C_\infty + Bx^\lambda, \tag{5}$$

where T_∞ and C_∞ are the temperature and concentration at infinity, respectively; A and B are constants > 0 for the heated plate, and λ is the power index of the wall temperature and concentration.

Equations (1)–(4) are subject to the following boundary conditions:

$$\begin{aligned} &v(x,0) = 0, \quad T(x,0) = T_w, \quad C(x,0) = C_w, \\ &u(x,\infty) = 0, \ T(x,\infty) = T_\infty, \ C(x,\infty) = C_\infty, \end{aligned} \tag{6}$$

where the Cartesian coordinates x and y are measured along the plate and along its normal, respectively (Fig. 1). The IHG and IMG rates are modeled from

$$q''' = \frac{\alpha(T_w - T_\infty)}{x^2} Ra_x^{2/3} e^{-\eta}, \quad q'''_m = \frac{D(C_w - C_\infty)}{x^2} Ra_x^{2/3} e^{-\eta}. \tag{7}$$

Then, Eqs. (1)–(5) admit the following similarity solutions:

$$\psi = \alpha Ra_x^{1/3} f(\eta), \quad \eta = Ra_x^{1/3} \left(\frac{y}{x}\right), \quad \theta(\eta) = \frac{T - T_\infty}{T_w - T_\infty}, \quad \phi(\eta) = \frac{C - C_\infty}{C_w - C_\infty}, \tag{8}$$

where $Ra_x = \frac{g\beta K(T_w - T_\infty)x}{\upsilon\alpha}$ is the modified local Rayleigh number.

The exponentially decaying IHG in Eq. (7) is extremely normal and was utilized as part of a request to acquire similarity solutions for the first time by Crepeau and Clarksean [11] for clear liquids and by

Postelnicu and Pop [12] for flows in permeable media. This IHG expression has since been utilized in various works.

Substituting Eqs. (6) and (8) into Eqs. (2)–(4) produces the following similarity equations:

$$\begin{aligned} &f''+\frac{\lambda-2}{3}\eta\left(\theta'+\mathrm{N}\phi'\right)+\lambda\left(\theta+\mathrm{N}\phi\right)=0,\\ &\theta''+\frac{\lambda+1}{3}f\theta'-\lambda f'\theta+ce^{-\eta}=0,\\ &\phi''-\mathrm{Le}\lambda\phi f'+\mathrm{Le}\left(\frac{\lambda+1}{3}\right)f\phi'+ce^{-\eta}=0, \end{aligned} \tag{9}$$

where a prime denotes ordinary differentiation with respect to η, and Le is the Lewis number,

$$\mathrm{Le}=\frac{\alpha}{D} \tag{10a}$$

and

$$\mathrm{N}=\frac{\beta_C(C_w-C_\infty)}{\beta_T(T_w-T_\infty)} \tag{10b}$$

is the sustentation parameter, which measures the relative importance of mass and thermal diffusion in the buoyancy-driven flow; β_T and β_C are the thermal and mass expansion coefficients, respectively; N is evidently positive for thermally assisted flows, zero for thermally driven flows, and negative for thermally opposing flows.

The transformed boundary conditions become the following:

$$\begin{aligned} &f(0)=0,\quad \theta(0)=1,\quad \phi(0)=1,\\ &f'(\infty)=0,\ \theta(\infty)=0,\ \phi(\infty)=0. \end{aligned} \tag{11}$$

The physical quantities of interest are the local Nusselt number, Nu_x, and the Sherwood number, Sh_x, which are defined, respectively, as follows:

$$Nu_x=\frac{xq_w}{k\left(T_w-T_\infty\right)},\quad Sh_x=\frac{xq_m}{D\left(C_w-C_\infty\right)},$$

where the heat transfer from the surface is given by the following: $q_m=-D\left(\frac{\partial C}{\partial y}\right)_{\text{at } y=0}$, and k is the thermal conductivity. Using the nondimensional variables (6), we obtain

$$Nu_x=-Ra_x^{1/3}\theta'(0)\quad\text{and}\quad Sh_x=-Ra_x^{1/3}\phi'(0). \tag{12}$$

3. RESULTS AND DISCUSSION

In the set boundary value problems in Eqs. (9) and (11) are solved with the use of the solve routine from Maple software, with the sustentation parameter N, exponent x^λ, and Lewis number Le as the prescribed parameters. Numerical results are plotted in Figs. 2–18, which exhibit the influences of the various parameters on the flow. Furthermore, the rates of heat transfer $-\theta'(0)$ and mass transfer $-\phi'(0)$ for nonzero values of the governing parameters are shown in Tables 1 and 2, respectively, with the maximum η value of 10.

Figures 2, 3, and 4 illustrate the effects of the sustentation parameter N on dimensionless velocity, temperature, and concentration profiles versus η, respectively, for the positive values of λ. In general, the fluid temperature is at its maximum on the plate surface and exponentially decreases to zero far away from the plate, thereby satisfying the boundary conditions. Figure 2 demonstrates that the thickness of

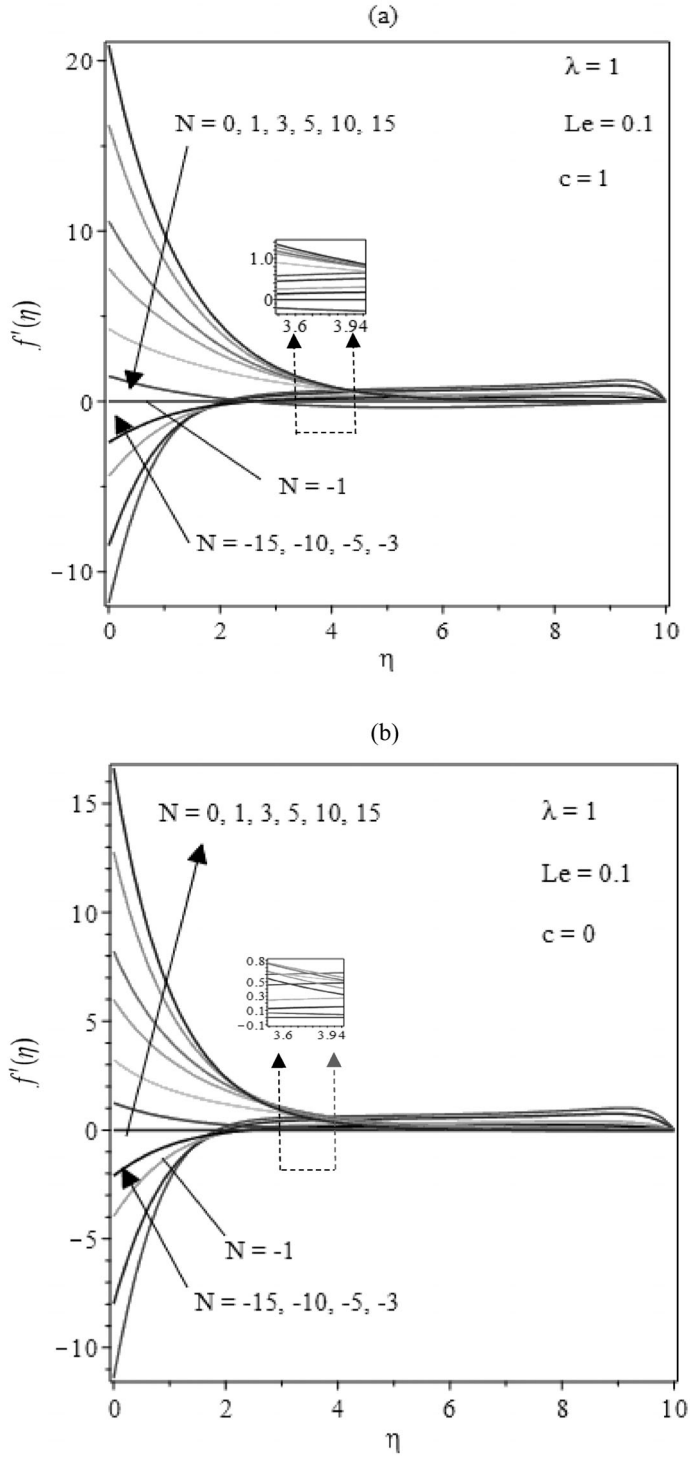

Fig. 2. Velocity profiles for different values of N: (a) with IHG and IMG, (b) without IHG and IMG.

the thermal boundary layer increases as $N > 0$ or $N < -1$. The flow is constant for $N = -1$. Notably, the flow is more significant with IHG and IMG than without them. By contrast, the thickness of the hydrodynamic boundary layer decreases as $N > 0$ or $N < -1$. For the positive values of the power law index λ ($\lambda = 1$), the temperature and concentration decrease with an increase in N, as shown in Fig. 3 and 4, respectively.

However, the velocity profile in Fig. 2 increases near the plate with N because the impact of the

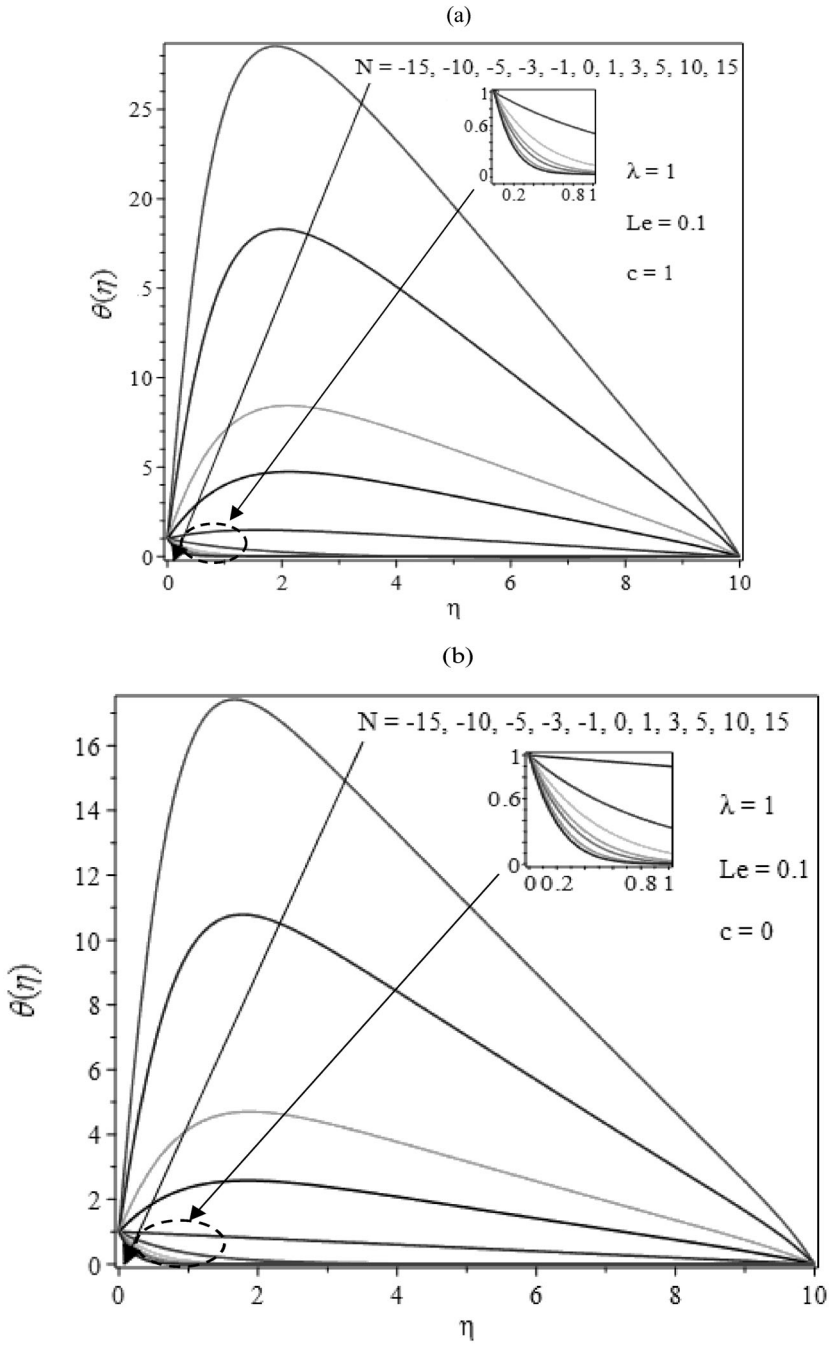

Fig. 3. Temperature profiles for different values of N: (a) with IHG and IMG, (b) without IHG and IMG with λ positive.

buoyancy ratio N expands the surface heat and mass transfer rates. Therefore, the concentration and the temperature gradient, and thus the heat and mass transfer rates, are expanded. The thermal boundary layer increases with the exponentially decaying IHG and IMG and decreases with an increase in the sustentation parameter N; that is, the temperature profile increases for $N \leq 0$ and decreases for $N > 0$. Figures 3 and 4 show that the temperature and concentration profile gradually decrease for $N \leq 0$ and rapidly for $N \geq 1$ for the cases with and without IHG and IMG. The opposite behavior is observed for the negative values of $\lambda(\lambda = -1/3)$, as shown in Fig. 5. For$\lambda = -1/3$, the positive values of N concentration profile increase more than those of λ, as shown in Fig. 6.

Figures 7, 8, and 9 analyze the influence of the diffusivity ratio Le on the dimensionless velocity,

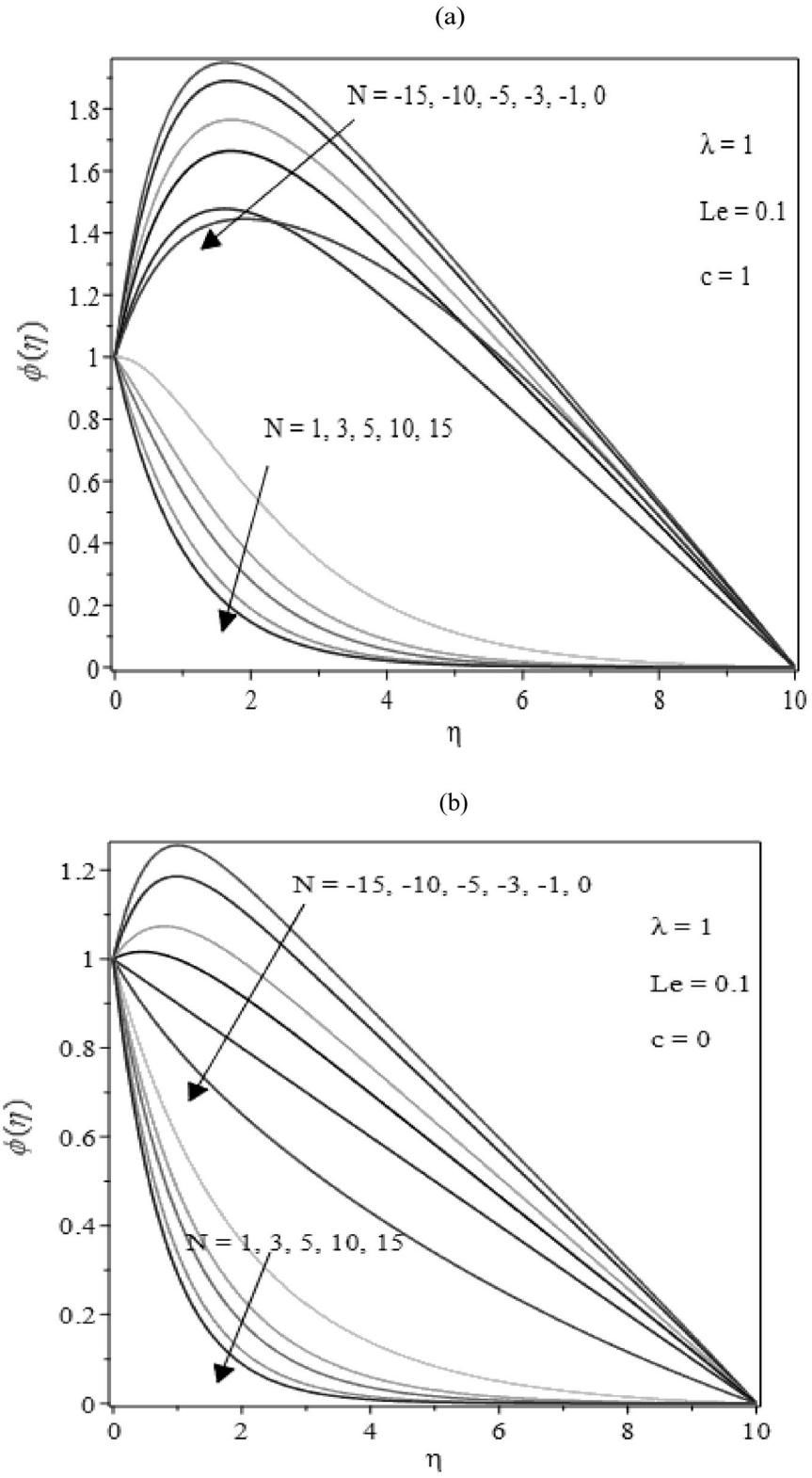

Fig. 4. Concentration profiles for different values of N: (a) with IHG and IMG, (b) without IHG and IMG with λ positive.

(a)

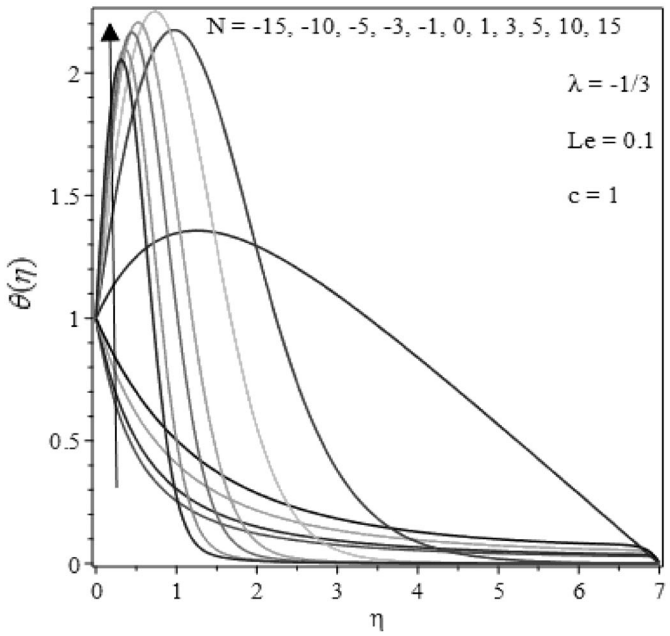

(b)

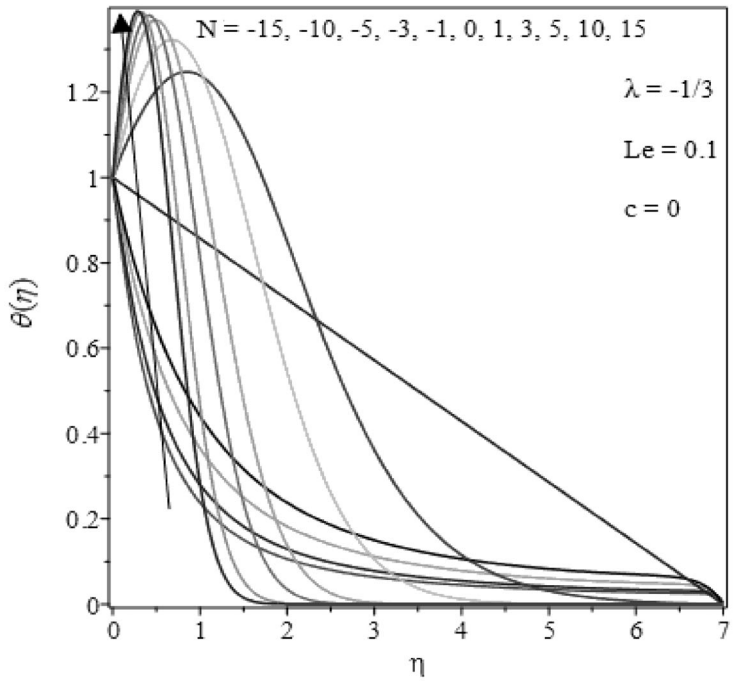

Fig. 5. Temperature profiles for different values of N: (a) with IHG and IMG, (b) without IHG and IMG with λ negative.

temperature, and concentration profile within the boundary layers, respectively. Le is a crucial parameter in changing the heat and mass transfer characteristics in the presence of IHG and IMG. The graphs in Fig. 7 show that an increase in the Lewis number, Le, leads to a fall in velocity distribution. Figures 8 and 9 demonstrate that as Le increases from 0.1 to 2, the temperature and concentration distribution increase for the fixed values of another parameter ($\lambda = 1$, $N = 10$). An opposite behavior is observed for $\lambda = -1/3$ and $N = 10$. Figures 7, 8, and 9 analyze the influence of the diffusivity ratio Le on the

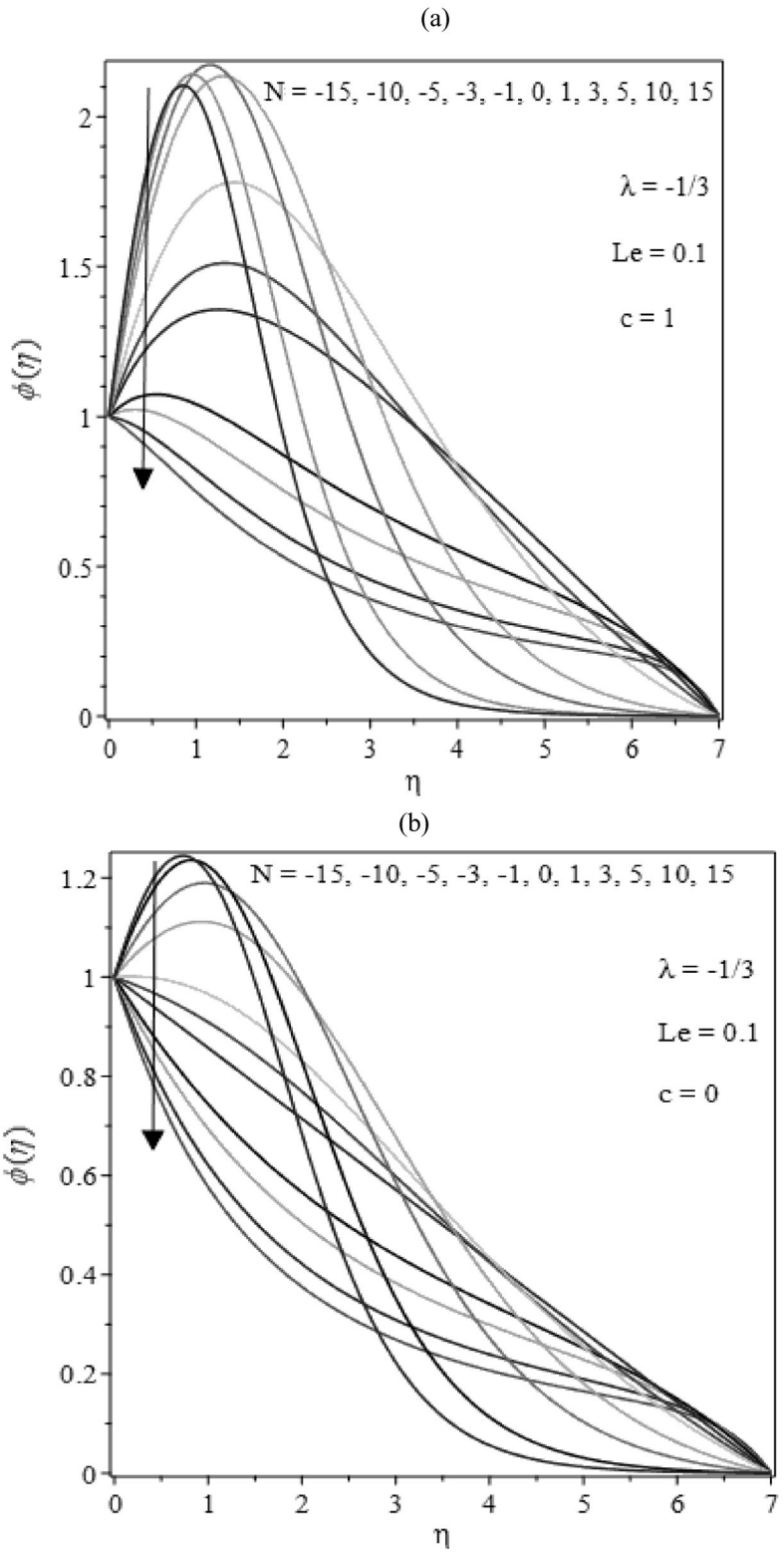

Fig. 6. Concentration profiles for different values of N: (a) with IHG and IMG, (b) without IHG and IMG with λ negative.

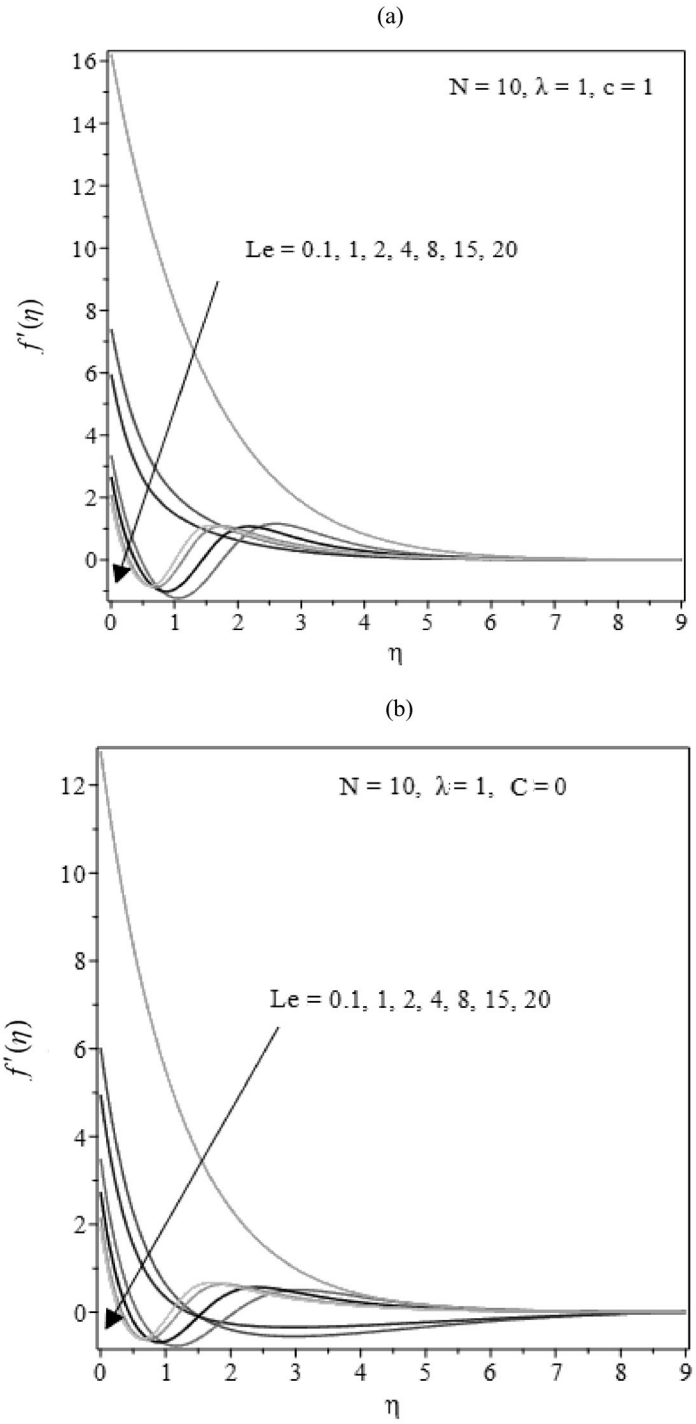

Fig. 7. Velocity profiles for different values of Le: (a) with IHG and IMG, (b) without IHG and IMG.

dimensionless velocity, temperature, and concentration profile within the boundary layers, respectively. The graphs in Fig. 7 show that an increase in the Lewis number Le leads to a fall in velocity distribution. Figures 8 and 9 demonstrate that as Le increases from 0.1 to 2, the temperature and concentration distribution increase for the fixed values of another parameter ($\lambda = 1$, $N = 10$). An opposite behavior is observed for $\lambda = -1/3$ and $N = 10$.

Figures 8 and 9 illustrate that for $Le = 4$, the temperature profile is overshooting positively and the

(a)

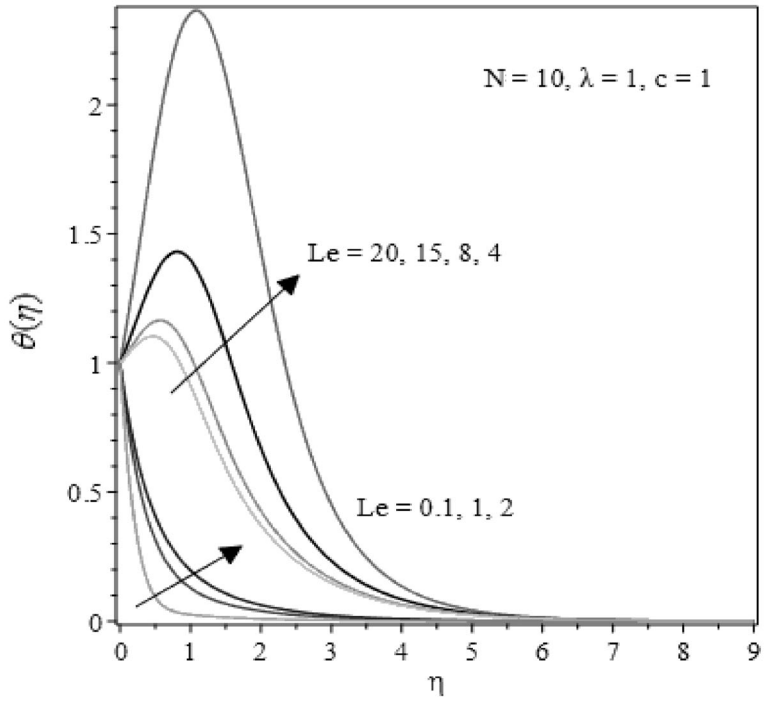

(b)

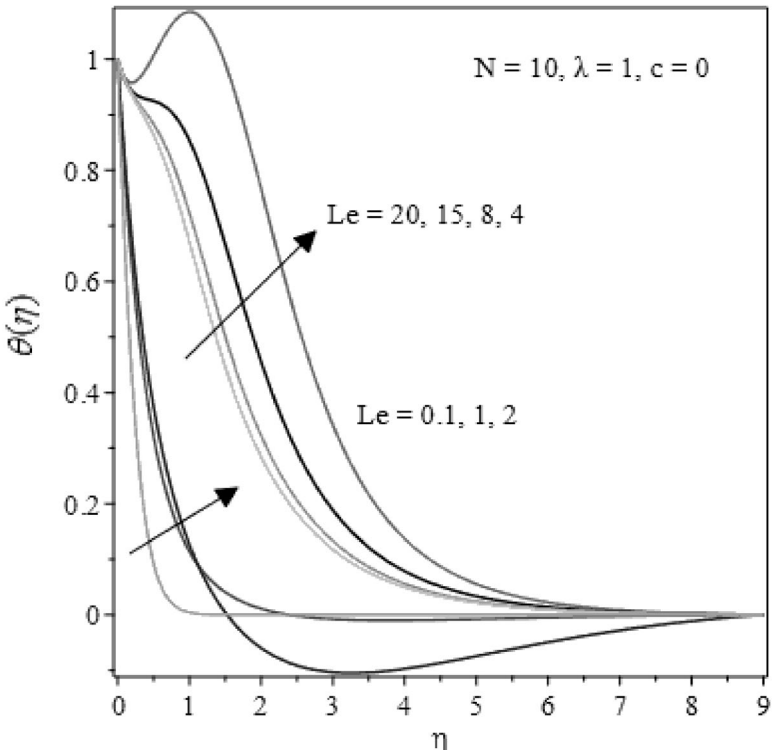

Fig. 8. Temperature profiles for different values of Le: (a) with IHG and IMG, (b) without IHG and IMG.

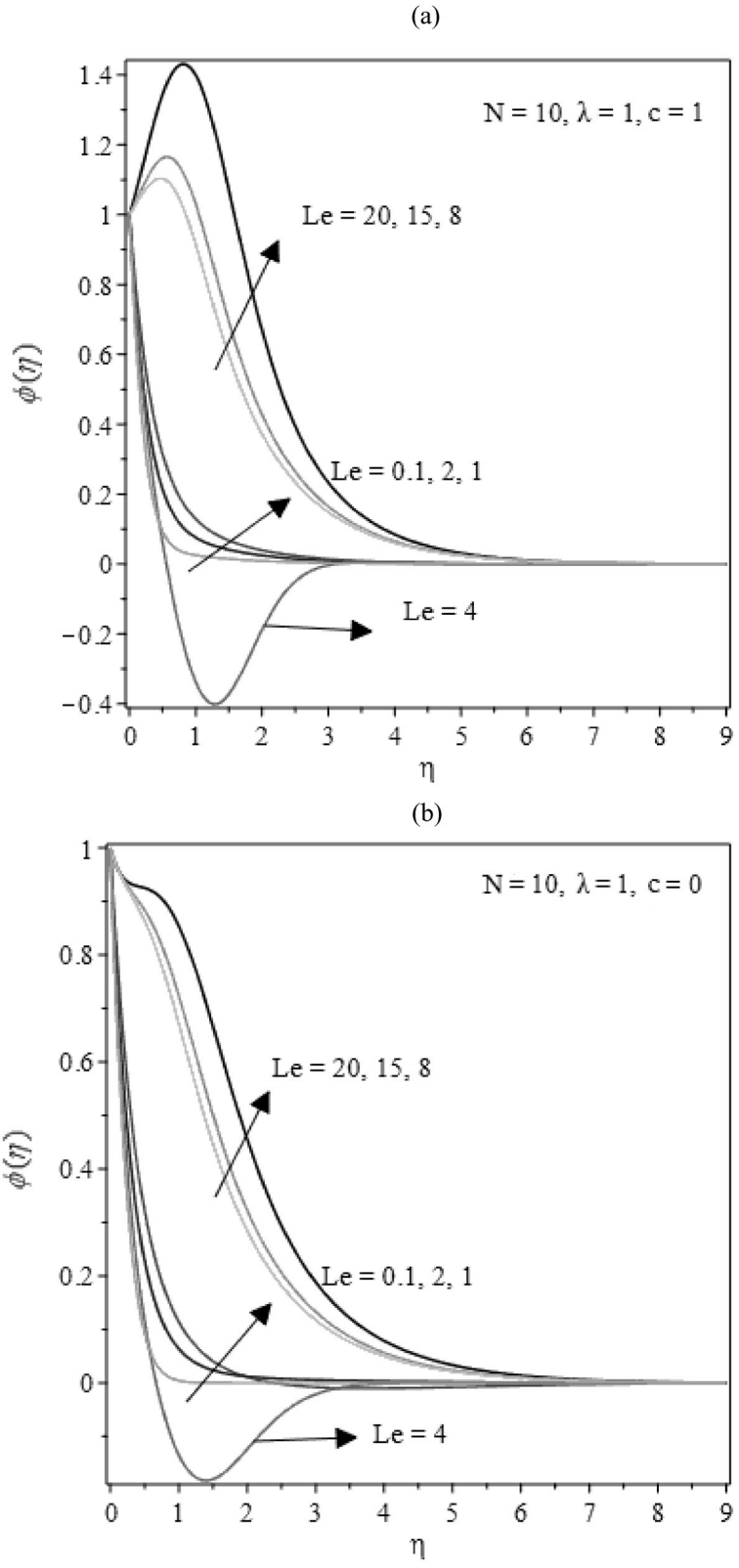

Fig. 9. Concentration profiles for different values of Le: (a) with IHG and IMG, (b) without IHG and IMG.

(a)

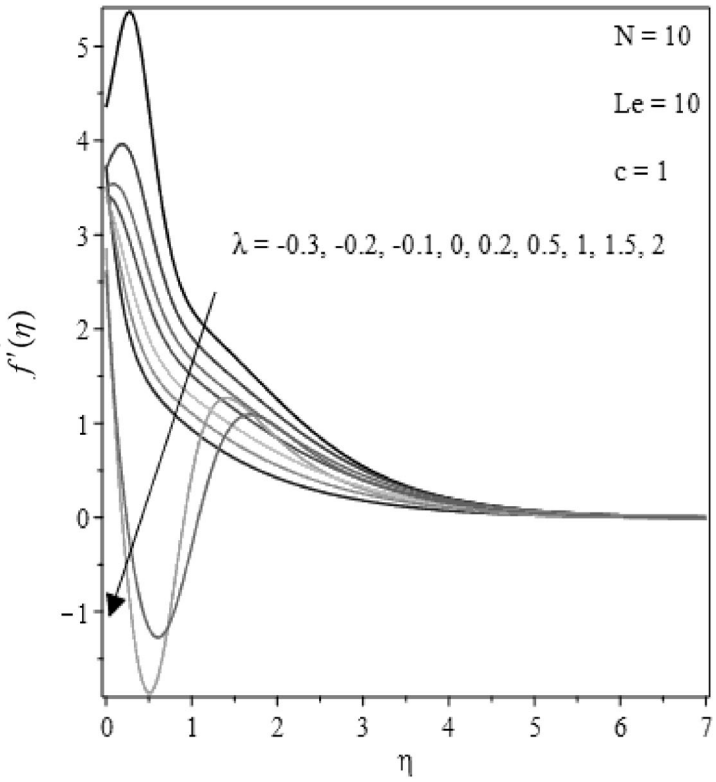

(b)

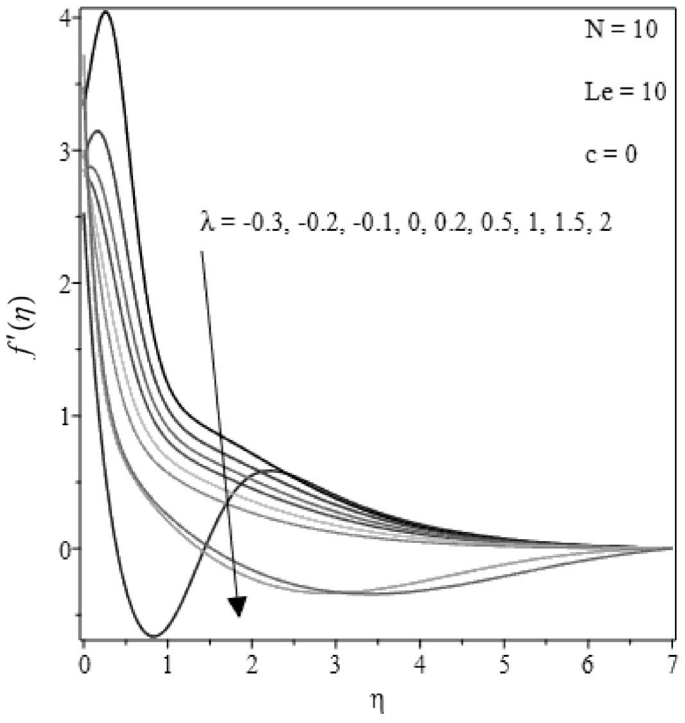

Fig. 10. Velocity profiles for different values of λ: (a) with IHG and IMG, (b) without IHG and IMG.

(a)

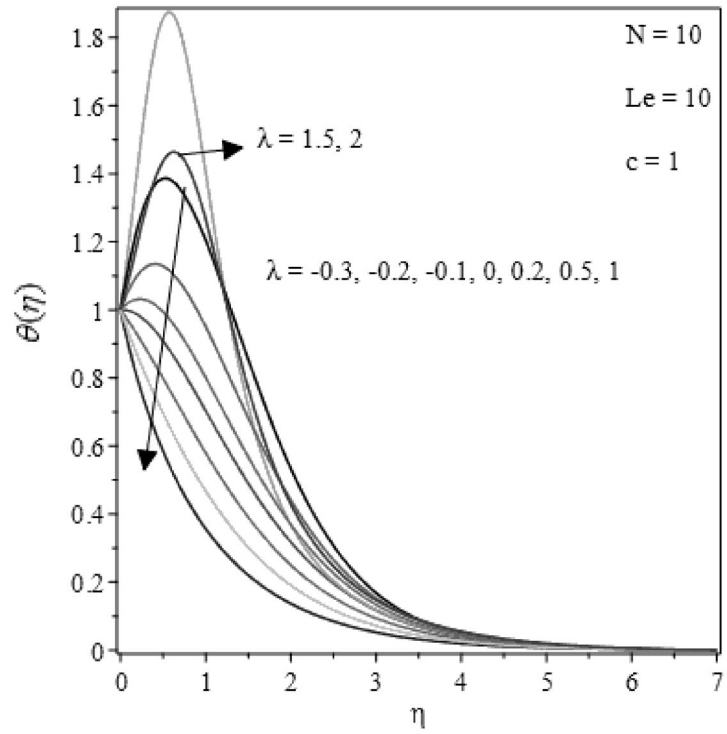

(b)

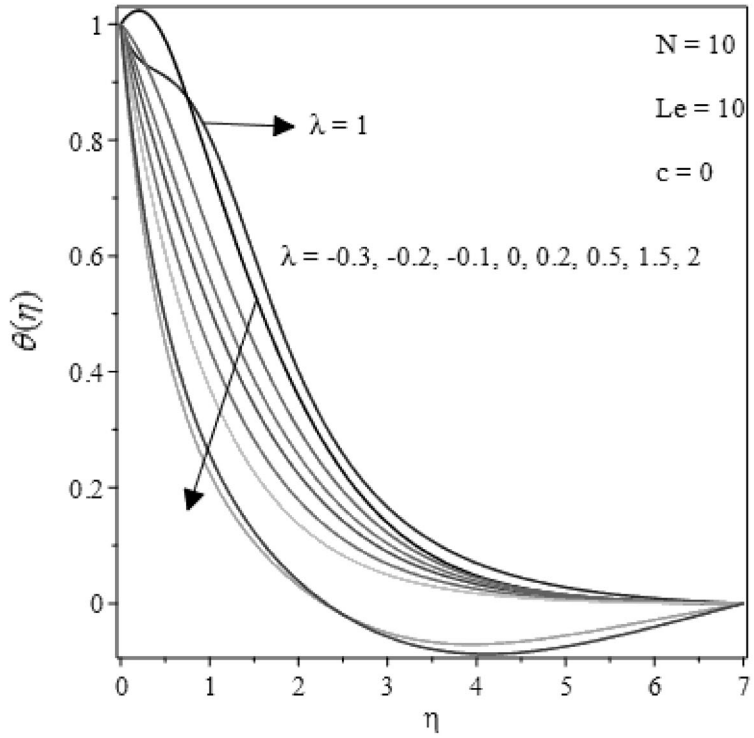

Fig. 11. Temperature profiles for different values of λ: (a) with IHG and IMG, (b) without IHG and IMG.

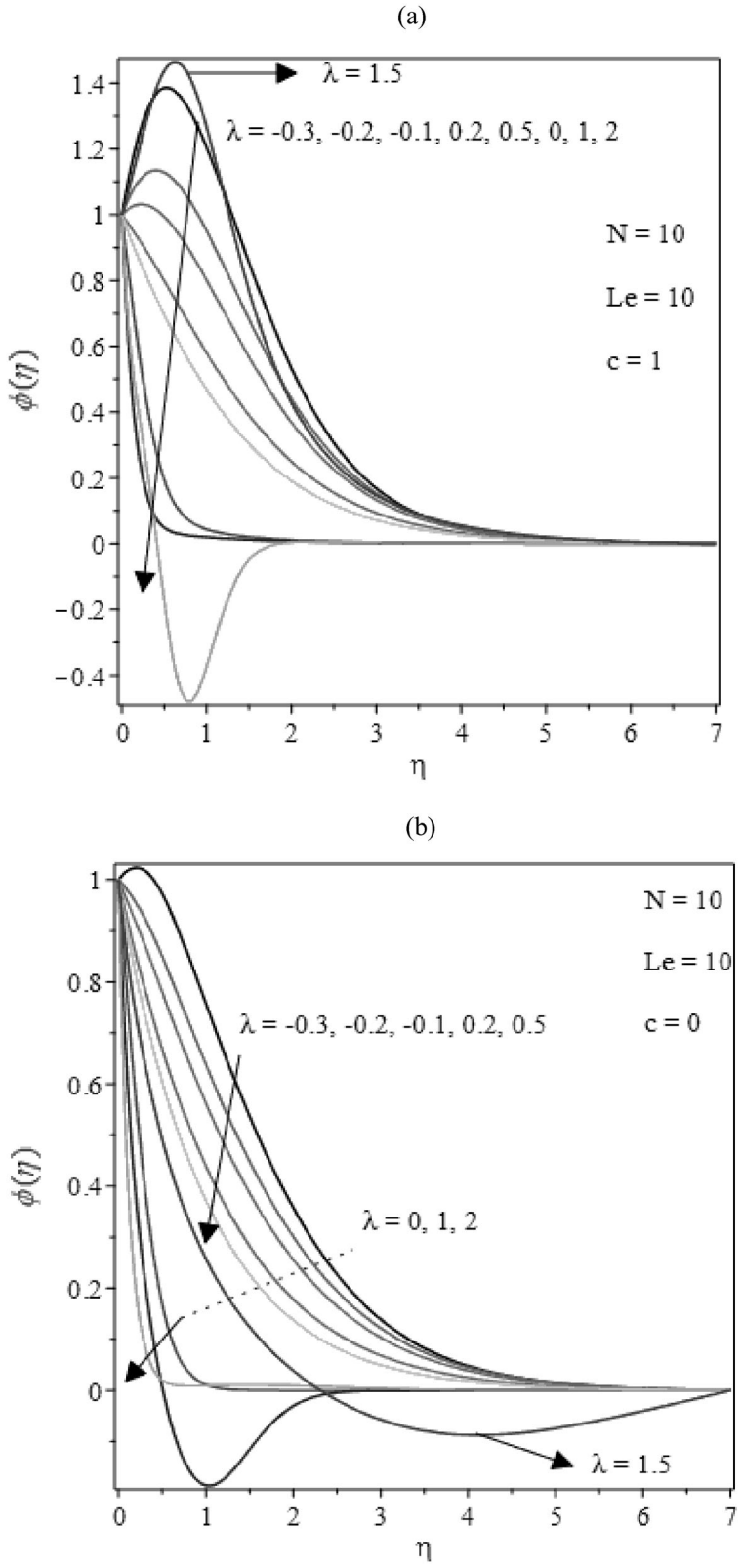

Fig. 12. Concentration profiles for different values of λ: (a) with IHG and IMG, (b) without IHG and IMG.

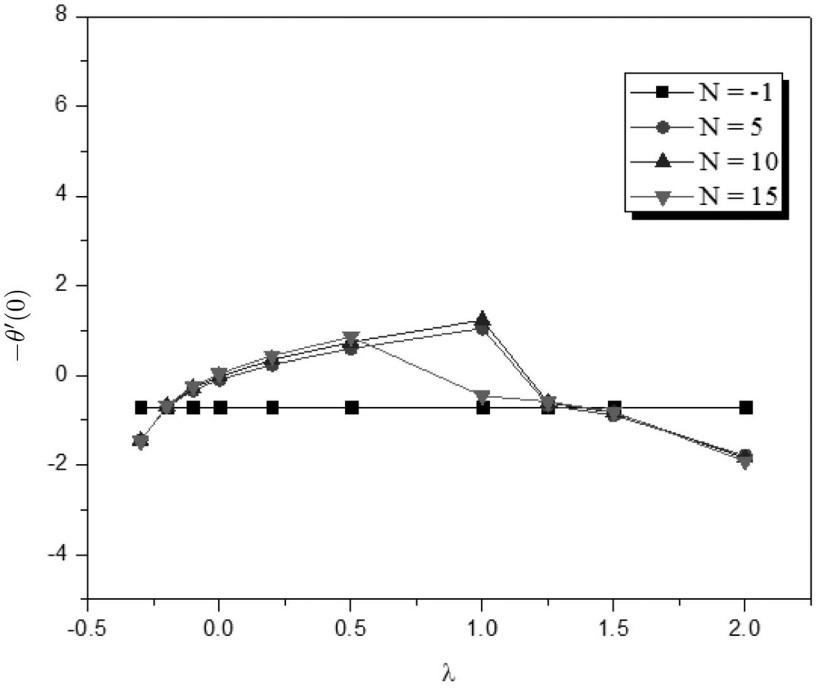

Fig. 13. Effects of N and λ on Nusselt number with fixed Le.

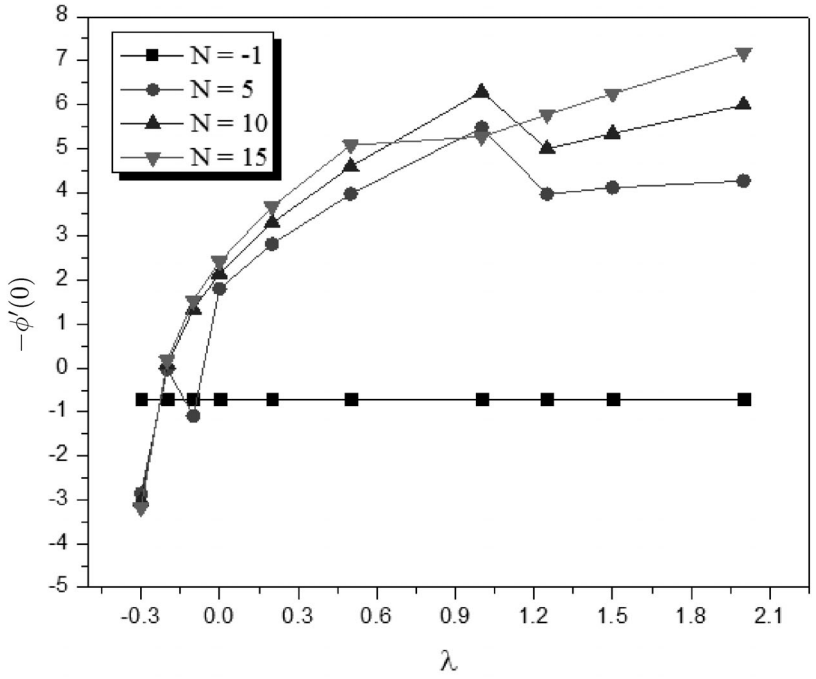

Fig. 14. Effects of N and λ on Sherwood number with fixed Le = 10.

concentration profile is decreasing negatively and then leads to zero with an increase in η because the heat transfer coefficient for Le = 4 is remarkably smaller than those of the other values of Le. For Le > 4, the temperature and concentration profile increase gradually. The behavior of Le with IHG and IMG and without them is the same.

Nondimensional velocity, temperature, and concentration profiles with IHG and IMG rates are shown

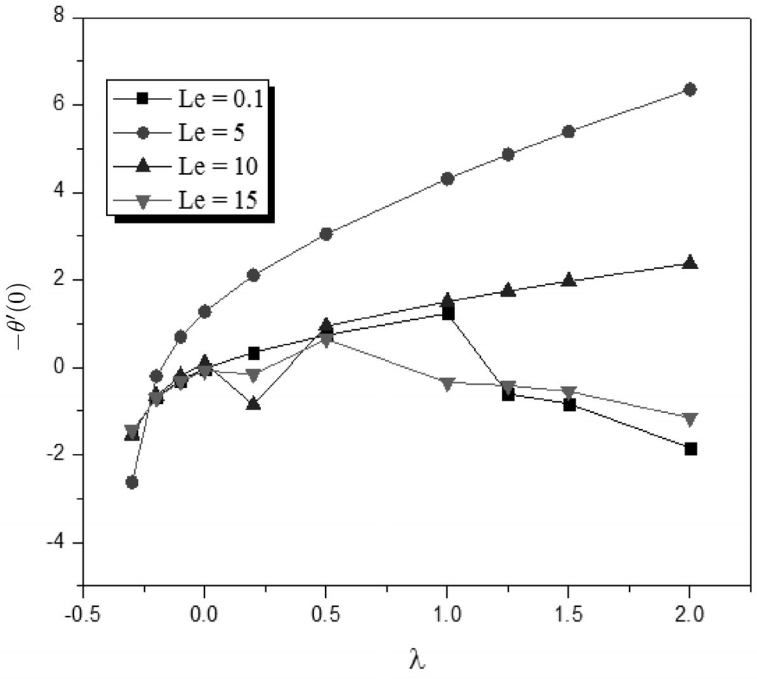

Fig. 15. Effects of Le and λ on Nusselt number with fixed N = 10.

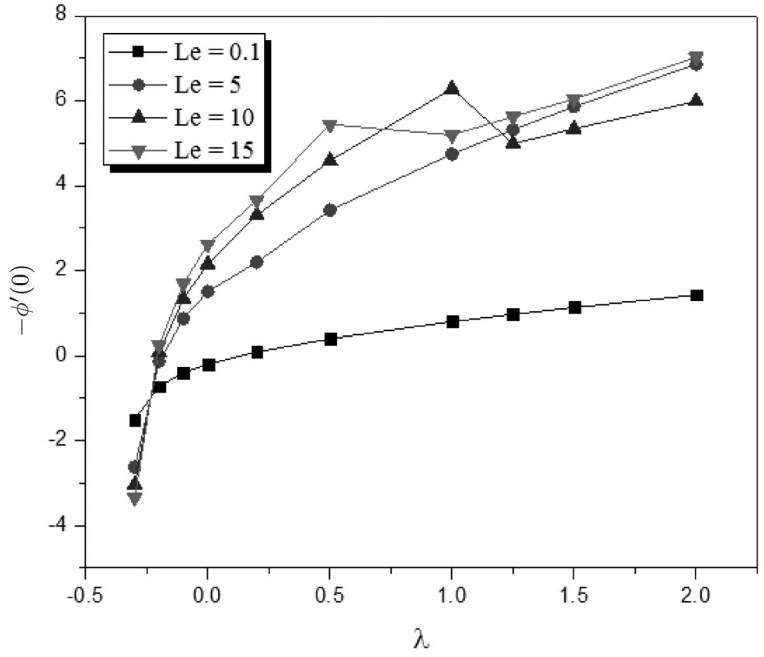

Fig. 16. Effects of Le and λ on Sherwood number with fixed N = 10.

for a few values of the temperature exponent λ in Figs. 10, 11, and 12, respectively. The plate is isothermal for $\lambda = 0$. The velocity profile decreases as the power law index λ increases in the cases with and without IHG and IMG. In the presence of IHG and IMG, the velocity profile for $\lambda > 1$ negatively decreases and then leads to zero with an increase in η.

Figure 11 demonstrates that heat and mass generation effects overshoot the temperature and concentration profiles close to the plate for $\lambda \leq 1$ and decrease with an increase in λ. However, the

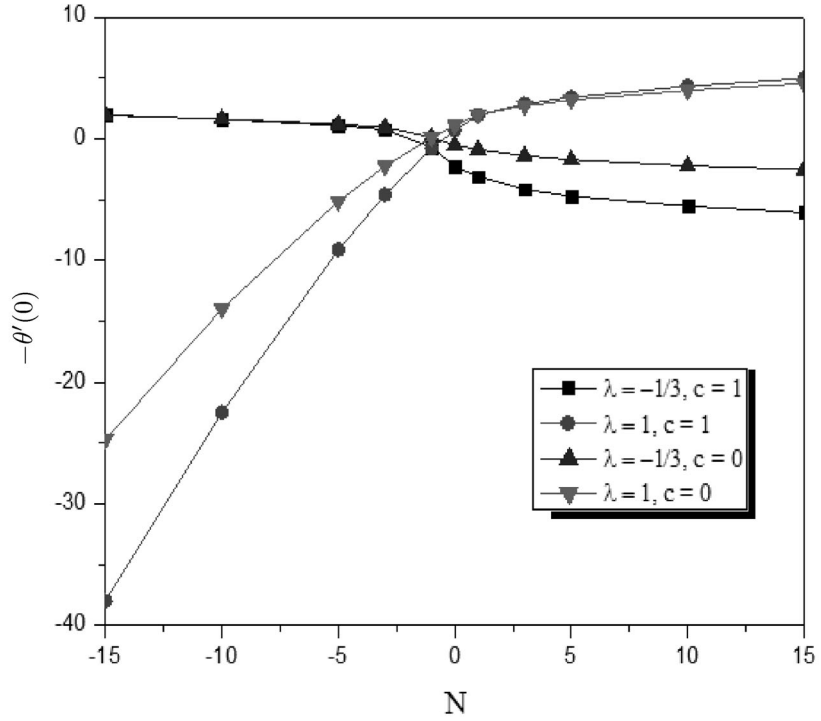

Fig. 17. Effects of λ and N on Nusselt number with fixed Le = 0.1.

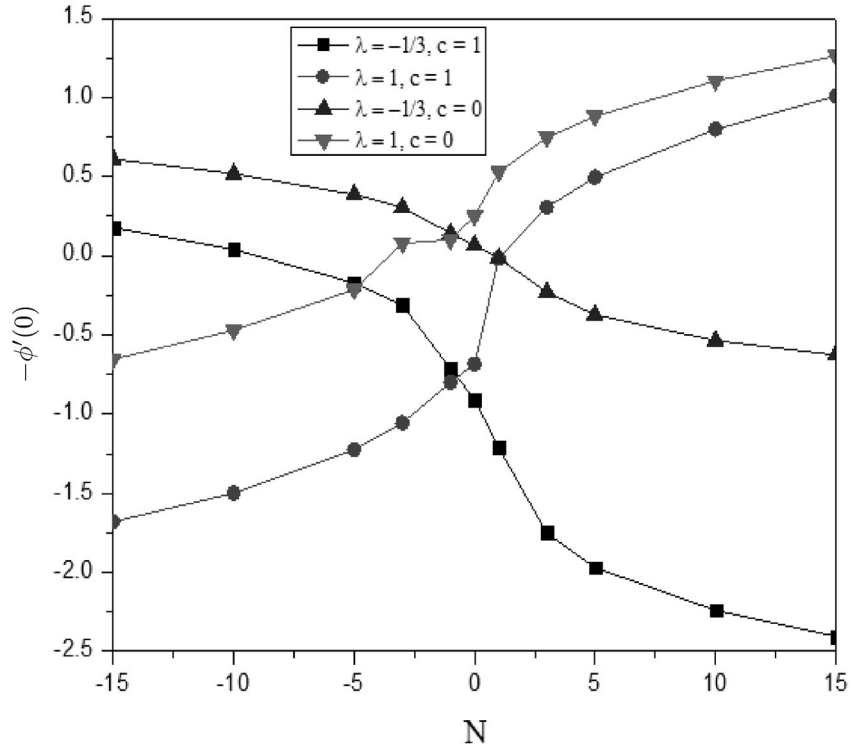

Fig. 18. Effects of λ and N on Sherwood number with fixed Le = 0.1.

temperature profile for $\lambda > 1$ is more pronounced than that for $\lambda \leq 1$. The opposite behavior is observed for $\lambda \geq 1$ without IHG and IMG.

Figures 13 and 14 represent the effects of the Nusselt and Sherwood numbers for λ for different values of N. For $N = -1$, the heat and mass transfer coefficient is constant. Increasing the sustentation parameter N increases the heat transfer coefficient up to $\lambda = 1$ and then suddenly decreases with the increase of λ. It is observed from Fig. 14 that Sherwood number sharply increases with the increase of N.

Figure 15 evidently shows that the heat transfer coefficient sharply increases for $Le = 5$. The parameter Le favors the magnitude of the mass transfer coefficient. Increasing Le with λ leads to an increase in the Sherwood number, as shown in Fig. 16.

Figures 17 and 18 indicate the effects of the buoyancy force, N and the power law index, λ, on the Nusselt and Sherwood numbers without IHG and IMG ($c = 0$) and with IHG and IMG ($c = 1$). Figure 17 shows that heat and mass transfer coefficients for a negative power law index value decrease

Table 1. Nondimensional heat transfer coefficients $-\theta'(0)$ for different values of λ and Le when $N = 10$ with IHG and IMG and without IHG and IMG

λ	Le	Without q''' $-\theta'(0)$	With q''' $-\theta'(0)$	Le	Without q''' $-\theta'(0)$	With q''' $-\theta'(0)$	Le	Without q''' $-\theta'(0)$	With q''' $-\theta'(0)$	Le	Without q''' $-\theta'(0)$	With q''' $-\theta'(0)$
$-1/3$	0.1	-2.11808	-5.44415	5	-0.56239	-2.08578	10	-0.42325	-1.87413	20	-0.35621	-1.81415
$-1/4$	0.1	-4.84422	-0.99271	5	0.00985	-0.98204	10	0.019267	-0.97437	20	0.02760	-0.96686
-0.19	0.1	0.53578	-0.09396	5	0.22929	-0.57986	10	0.20314	-0.62361	20	0.08996	-0.64558
-0.15	0.1	0.78995	0.29707	5	0.34019	-0.38659	10	0.29780	-0.45292	20	0.27384	-0.49023
-0.1	0.1	1.04994	0.676631	5	0.45539	-0.19345	10	0.39698	-0.28144	20	0.36195	-0.33448
0	0.1	1.46572	1.24905	5	0.63879	0.09896	10	0.55605	-0.02085	20	0.50382	-0.09788
1/4	0.1	2.24746	2.25002	5	0.62313	0.58927	10	0.84435	0.41652	20	0.76264	0.30009
1/3	0.1	2.46877	2.522190	5	1.05890	0.71660	10	0.92271	0.52995	20	0.83335	0.403590
1/2	0.1	2.87904	3.018237	5	1.221595	0.94314	10	1.064730	0.73155	20	1.287842	1.039919
3/4	0.1	3.43952	3.68242	5	-1.43772	1.23785	10	1.25341	0.99348	20	1.13300	0.827515
1	0.1	3.95571	4.28369	5	1.63255	1.49878	10	1.42340	1.22518	20	1.28784	1.039919

Table 2. Nondimensional mass transfer coefficients for different values of λ and Le when $N = 10$ with IHG and IMG and without IHG and IMG

λ	Le	Without q''' $-\phi'(0)$	With q''' $-\phi'(0)$	Le	Without q''' $-\phi'(0)$	With q''' $-\phi'(0)$	Le	Without q''' $-\phi'(0)$	With q''' $-\phi'(0)$	Le	Without q''' $-\phi'(0)$	With q''' $-\phi'(0)$
$-1/3$	0.1	-0.40445	-2.12388	5	-2.2749	-4.99956	10	-2.96642	-6.02953	20	-3.89109	-7.41437
$-1/4$	0.1	0.04161	-0.95342	5	3.31846	-0.99239	10	-5.86642	-0.99278	20	-1.69169	-0.99301
-0.19	0.1	0.17928	-0.65804	5	0.64234	-0.00426	10	0.840254	0.24704	20	1.104731	0.576295
-0.15	0.1	0.24716	-0.52485	5	0.94689	0.43991	10	1.239093	0.79824	20	1.629786	1.274445
-0.1	0.1	0.31759	-0.39431	5	1.25561	0.86217	10	1.643758	1.33496	20	2.163132	1.955764
0	0.1	0.43105	-0.19781	5	1.74057	1.50169	10	2.280280	2.14092	20	3.003547	2.983432
1/4	0.1	0.643103	0.137208	5	2.45216	2.59430	10	3.438977	3.52708	20	4.537826	4.766789
1/3	0.1	0.702535	0.225967	5	2.86505	2.88572	10	3.759467	3.89871	20	4.962933	5.248066
1/2	0.1	0.812085	0.385548	5	3.31146	3.41191	10	4.347168	4.57419	20	5.742929	6.121970
3/4	0.1	0.960787	0.595778	5	3.91390	4.10882	10	5.140120	5.46511	20	6.795748	7.287321
1	0.1	1.097148	0.78372	5	4.46421	4.73452	10	5.863615	6.26960	20	7.756338	8.339652

from positive to negative. However, heat and mass transfer coefficients increase when the power law index, λ, is positive.

The effects of controlling parameters λ and Le on the rates of dimensionless heat transfer $-\theta'(0)$ (local Nusselt number) and mass transfer $-\phi'(0)$ (local Sherwood number) with and without IHG and IMG are shown in Tables 1 and 2, respectively.

The tables show that as the power law index λ increases, the rates of heat transfer $-\theta'(0)$ and mass transfer $-\phi'(0)$ increase. The local Nusselt number reacts negatively when Le is increased. However, the mass transfer rate at the surface increases with Le for $\lambda \geq -0.3$. The solution for $\lambda < -0.3$ does not exist for this problem. The negative value of the Sherwood number implies that the surface is losing mass. The thermal boundary layer thickness increases while the concentration boundary layer decreases as Le is increased, thereby causing this effect. These behaviors are more significant with IHG and IMG than without them.

4. CONCLUSIONS

In the presence of exponentially decaying IHG and IMG over a specific component, a steady, laminar, and viscous flow model was developed for the free convective heat and mass transfer from a vertical surface embedded in a porous medium. The governing nonlinear ordinary differential equations were numerically solved with the use of quadrature functions in Maple. The following are the important findings:

- In this model, we showed that a similarity solution exists for an extensive range of values of λ while a solution does not exist for $\lambda < -0.3$.
- Our investigation of the effects of the Lewis number on the velocity and the temperature and concentration profiles has indicated that the velocity profile decreases as the Lewis number increases. The heat and mass transfer coefficients decrease and increase for a wide range of Lewis numbers.
- The thickness of the momentum and thermal boundary layers increases as the sustentation parameter N increases or decreases. This behavior is more significant with IHG and IMG than without them.
- Exponentially decaying IHG and IMG over a specific component model can be used in mixtures where a radioactive material is surrounded by inert alloys. This model has been adopted to demonstrate the electromagnetic heating of materials. Extension of this model is recommended for an extensive range of λ values, such as $\lambda < -0.3$.

REFERENCES

1. Nield, A.D. and Bejan, A., *Convection in Porous Media*, New York: Springer, 1999, Chapter 5.
2. Ingham, D.B. and Pop, I., *Transfer Phenomena in Porous Media*, Oxford: Pergamon, 1998.
3. Cheng, P. and Minkowycz, W.J., Free Convection about a Vertical Flat Plate Embedded in a Porous Medium with Application to Heat Transfer from a Dike, *J. Geophys. Res.*, 1977, vol. 82, no. 14, pp. 2040–2044.
4. Cheng, P., The Influence of Lateral Mass Flux on Free Convection Boundary Layers in a Saturated Porous Medium, *Int. J. Heat Mass Transfer*, 1977, vol. 20, pp. 201–206.
5. Johnson, C.H. and Cheng, P., Possible Similarity Solutions for Free Convection Boundary Layers Adjacent to Flat Plates in Porous Media, *Int. J. Heat Mass Transfer*, 1978, vol. 21, pp. 709–718.
6. Chaudhary, M.A., Merkin, J.H., and Pop, I., Similarity Solutions in Free Convection Boundary Layer Flows Adjacent to Vertical Permeable Surfaces in Porous Media, I: Prescribed Surface Temperature, *European J. Mech. Fluids*, 1995, vol. 14, pp. 217–237.
7. Chaudhary, M.A., Merkin, J.H., and Pop, I., Similarity Solutions in Free Convection Boundary Layer Flows Adjacent to Vertical Permeable Surfaces in Porous Media, II: Prescribed Surface Heat Flux, *Heat Mass Transfer*, 1995, vol. 30, pp. 341–347.
8. Wright, S.D., Ingham, D.B., and Pop, I., On Natural Convection from a Vertical Plate with a Prescribed Surface Heat Flux in Porous Media, *Trans. Porous Media*, 1996, vol. 22, pp. 181–193.
9. Ingham, D.B. and Brown, I.N., Flow past a Suddenly Heated Vertical Plate in a Porous Medium, *Proc. Roy. Soc. London, Ser.* A, 1986, vol. 403, pp. 51–80.
10. Magyari, E. and Keller, B., Exact Analytical Solutions for Free Convection Boundary Layers on a Heated Vertical Plate with Lateral Mass Flux Embedded in a Saturated Porous Medium, *Heat Mass Transfer*, 2000, vol. 36, pp. 109–116.

11. Crepeau, J.C. and Clarksean, R., Similarity Solutions of Natural Convection with Internal Heat Generation, *ASME J. Heat Transfer*, 1997, vol. 119, pp. 183–185.
12. Postelnicu, A. and Pop, I., Similarity Solutions of Free Convection Boundary Layers over Vertical and Horizontal Surfaces in Porous Media with Internal Heat Generation, *Int. Comm. Heat Mass Transfer*, 1999, vol. 26, no. 8, pp. 1183–1191.
13. Postelnicu, A., Grosan, T., and Pop, I., Free Convection Boundary Layer over a Vertical Permeable Flat Plate in a Porous Medium with Internal Heat Generation, *Int. Comm. Heat Mass Transfer*, 2000, vol. 27, no. 5, pp. 729–738.
14. Grosan, T. and Pop, I., Free Convection over a Vertical Plate with Variable Wall Temperature and Internal Heat Generation in Porous Medium Saturated with a Non-Newtonian Fluid, *Tech. Mech.*, 2001, vol. 21, pp. 313–318.
15. Grosan, T. and Pop, I., Free Convection of Non-Newtonian Fluids over a Vertical Surface in a Porous Medium with Internal Heat Generation, *Int. J. Appl. Mech. Engrg.*, 2002, vol. 7, pp. 401–407.
16. Bagai, S., Similarity Solutions of Free Convection Boundary Layers over a Body of Arbitrary Shape in a Porous Medium with Internal Heat Generation, *Int. Comm. Heat Mass Transfer*, 2003, vol. 30, no. 7, pp. 997–1003.